Joint Frequency and 2-D DOA Recovery with sub-Nyquist Difference Space-Time Array

A Anil Kumar, M Girish Chandra and P Balamuralidhar
TCS Research and Innovation, Bangalore, India.
Email:{achannaanil.kumar, m.gchandra, balamurali.p}@tcs.com.

***Abstract*—In this paper, joint frequency and 2-D direction of arrival (DOA) estimation at sub-Nyquist sampling rates of a multi-band signal (MBS) comprising of P disjoint narrowband signals is considered. Beginning with a standard uniform rectangular array (URA) consisting of $M = M_x \times M_y$ sensors, this paper proposes a simpler modification by adding a $N-1$ delay channel network to only one of the sensor. A larger array is then formed by combining the sub-Nyquist sampled outputs of URA and the delay channel network, referred to as the difference space-time (DST) array. Towards estimating the joint frequency and 2-D DOA on this DST array, a new method utilizing the 3-D spatial smoothing for rank enhancement and a subspace algorithm based on ESPRIT is presented. Furthermore, it is shown that an ADC sampling frequency of $f_s \geq B$ suffices, where B is the bandwidth of the narrow-band signal. With the proposed approach, it is shown that $\mathcal{O}(MN/4)$ frequencies and their 2-D DOAs can be estimated even when all frequencies alias to the same frequency due to sub-Nyquist sampling. Appropriate simulation results are also presented to corroborate these findings.**

***Index Terms*—Joint frequency-direction of arrival estimation, sub-Nyquist sampling, Space-time array, ESPRIT, Uniform rectangular array, Multiple-delay architecture.**

I. Introduction

Of late, the quest for improving the degrees of freedom with fewer physical elements has drawn considerable attention. Primarily, this is motivated by the fact that over recent years, although the cost of physical elements such as sensors have come down, the deployment (which requires several additional components) and the maintenance cost is still higher. Encouraged by these recent developments, in this paper we consider the important problem of *joint frequency and 2-D DOA* (i.e., azimuth and elevation) estimation of multi-band signal (MBS) (i.e., multiple disjoint narrow band signals spread within the wide spectrum), under the scenario where the *number of sources can exceed the number of sensors*. This typically find applications in cognitive radio (CR) [1], radar, communications ([2], [3]) etc. Further, it has also been well established that in these applications a wide spectrum has to be sensed [4]. Thus, it is not only important but essential to estimate these parameters at *sub-Nyquist sampling rates*; which not only eliminates the necessity of high sampling rate ADC, but also overcomes the subsequent high rate operations.

In literature, many methods such as [5] - [9] have been proposed for frequency and DOA estimation at sub-Nyquist sampling rates for the case of $M > P$, where M and P denotes the number of sensors and sources respectively. Based on the above methods and the recent advancements in array processing and sub-Nyquist sampling schemes, [10] - [12] proposed methods to address the case of $M < P$. While [10] employed a nested sensor array [13] based architecture, [11] and [12] considered to use a multi-coset sub-Nyquist sampler [14] at the output of every sensor. In practice, a multi-coset receiver is realized through a multi-channel architecture and hence requires more hardware channels to implement the methods of [11], [12]. Thus, for the problem considered in this paper, the existing methods either requires a newer array geometry or would require more hardware.

In this paper, we assume a standard uniform rectangular array (URA) configuration and propose an efficient method for joint frequency and 2-D DOA estimation for the case of $M < P$ at sub-Nyquist sampling rates. Based on the idea of [8], the architecture is suitably modified by adding a $N-1$ channel delay network at only one sensor. By assuming the sources to be uncorrelated, we describe a process for obtaining a larger array referred as the *Difference Space Time* (DST) array. Although URA is a 2-D uniform array, this DST array would be a *3-D uniform array*; two dimensions corresponding to spatial delay and the third dimension corresponding to a temporal delay. With this modification, a new rank enhancement method and a corresponding estimation algorithm based on ESPRIT [15] is presented for estimating automatically paired parameters. Later in Section III-D we show that with the proposed approach and for a URA comprising of $M = M_x \times M_y$ sensors and a single $N-1$ channel delay network (number of ADC channels = $M + N - 1$), upto $P \leq M(N-1)/4$ carrier frequencies and their 2-D DOAs can be determined. Further, it will be shown that if the bandwidth of the narrow-band signal does not exceed B, then a minimum overall sampling rate of $(M+N-1)B$ would be sufficient to estimate the above mentioned number of carrier frequencies and their 2-D DOAs which shall also be corroborated through simulation results.

II. Signal model and Problem description

We assume P uncorrelated, disjoint, far-field, narrow-band signals which are spread within a wide spectrum of $\mathcal{F} = [0, 1/T]$, impinging on a URA comprising of $M = M_x \times M_y$ omnidirectional sensors. Let $x(t)$ denote the combination of P narrow-band signals referred to as multi-band signal (MBS), which can be expressed as

$$x(t) = \sum_{p=1}^{P} s_p(t) e^{j2\pi f_p t} \tag{1}$$

ISBN 978-0-9928626-7-1

where $s_p(t), 1 \leq p \leq P$ denotes the p^{th} narrow-band source signal whose bandwidth doesn't exceed B, and further $B \ll 1/T$. $\{f_p\}_{p=1}^{P}$ denotes the unknown carrier frequencies that are spread within $\mathcal{F}$. Further, the disjoint band assumption implies that the unknown carrier frequencies are distinct i.e.,$f_{p_1} \neq f_{p_2}$, for all $p_1 \neq p_2$ and $1 \leq p_1, p_2 \leq P$. Since the carrier frequencies are unknown, the Nyquist sampling rate of $x(t)$ is $f_{nyq} = 1/T$. Let us assume a symmetric URA whose sensor array locations are given by

$$\mathcal{S}_{ura} = \{d\mathbf{I}[m_x \quad m_y], -\lfloor M_x/2 \rfloor \leq m_x \leq \lceil M_x/2 \rceil - 1, \\ -\lfloor M_y/2 \rfloor \leq m_y \leq \lceil M_y/2 \rceil - 1\} \quad (2)$$

where $\mathbf{I}$ denotes the identity matrix, $m_x, m_y \in \mathbb{Z}$ and $d \leq c/2T$; c is the wave propagation velocity. Now, the signal observed by the above URA can be expressed in the following form as

$$\mathbf{x}_s(t) = \underbrace{(\mathbf{A}_x \odot \mathbf{A}_y)}_{\mathbf{A}_s} \mathbf{s}(t) + \boldsymbol{\eta}(t) \quad (3)$$

where the spatial array manifold matrices for $k = x$ and $k = y$, $\mathbf{A}_k = [\mathbf{a}_k(f_1, \theta_1, \phi_1), ..., \mathbf{a}_k(f_P, \theta_P, \phi_P)]$ and $\mathbf{a}_k(f_p, \theta_p, \phi_p) = [e^{j2\pi(d/c)\lfloor M_k/2 \rfloor \omega_p^k}, ...1, ..., e^{-j2\pi(\lceil M_k/2 \rceil - 1)(d/c)\omega_p^k}]^{\mathcal{T}}$, $\mathbf{s}(t) = [s_1(t)e^{j2\pi f_1 t}, ..., s_P(t)e^{j2\pi f_P t}]^{\mathcal{T}}$, $\omega_p^x = f_p \cos\theta_p \sin\phi_p$ and $\omega_p^y = f_p \sin\theta_p \sin\phi_p$. $\{\theta_p, \phi_p\}_{p=1}^{P}$ denotes the 2-D DOA of the p^{th} source, d denotes the distance between the adjacent elements both along x-axis as well as along y-axis and $\boldsymbol{\eta}(t)$ denotes the noise vector which is white and uncorrelated with the signal. Let us sample $\mathbf{x}_s(t)$ at a sub-Nyquist sampling rate of $f_s = 1/LT$ i.e., the ADCs samples at every $t = nLT$, where L denotes the sub-sampling factor. The sub-sampled signal $\mathbf{x}_s(n)$ can be expressed as

$$\mathbf{x}_s(n) = \mathbf{A}_s \mathbf{s}(n) + \boldsymbol{\eta}(n). \quad (4)$$

Now, the discrete time Fourier transform (DTFT) of $\mathbf{x}_s(n)$, $\mathbf{X}_s(f)$ can be expressed as [7]

$$\mathbf{X}_s(f) = \mathbf{A}_s \mathbf{S}(f) + \boldsymbol{\eta}(f) \quad (5)$$

where $\mathbf{S}(f) = [S_1(f), S_2(f), ..., S_P(f)]^{\mathcal{T}}$, $S_p(f)$ denotes the periodic *aliased spectrum* of the p^{th} source signal.

As mentioned earlier, $x(t)$ is assumed to be a wideband signal and hence $1/T$ will be a large quantity and hence sampling at Nyquist rate may not be feasible. Thus the aim of this paper is to estimate the parameters $\{f_p, \theta_p, \phi_p\}_{p=1}^{P}$ at sub-Nyquist sampling under the scenario that the number of sources can exceed the number of sensors i.e., $P > M$. Further we would like to achieve the above stated goals without enormously increasing the hardware complexity.

Now, observe from $\{\omega_p^x, \omega_p^y\}_{p=1}^{P}$, that the carrier frequencies and DOAs appear in non-separable form and estimating the triple $\{f_p, \theta_p, \phi_p\}_{p=1}^{P}$ from these two quantities is not possible. Further, the signal is sampled at sub-Nyquist sampling rates making it difficult to estimate the carrier frequencies from the sub-sampled $x(n)$. Hence, besides suitably modifying the architecture which can aid in estimating the carrier frequencies, the recovery approach must also facilitate joint estimation of these parameters in order to overcome the association problem. The following section describes the proposed approach for achieving the above stated goals.

III. Proposed Method

We begin the description of the proposed approach by briefly describing the modified architecture based on multiple delay architecture of [8] and the process of obtaining the DST array is then outlined. Followed by this, we provide the details of the estimation algorithm for estimating automatically paired parameters.

A. Multiple Delay Architecture

Recall from the previous section that URA is symmetric (see (2)). The receiver architecture is modified by adding an $N-1$ channel delay network $\{q\tau T\}_{q=1}^{N-1}$ to the sensor placed at the origin as shown in Fig. 1. The delay factor can be in the range $0 < \tau \leq 0.5$. In order to minimize the hardware complexity, *the delay network is added only to one sensor*. All the ADCs are synchronized and they sample at a sub-Nyquist sampling rate of $f_s = 1/LT$. As also observed in [8] the delay network can easily be realized by a simple cascaded network comprising of N *identical delay* elements, which forms the key attractive feature compared to the architectures of [11], [12]. Let $x_q^d(t)$, $q = \{1, 2, ..., N-1\}$ be the signal corresponding to the q^{th} *temporal* delay channel, which can be expressed as (using (1))

$$\begin{aligned} x_q^d(t) &= \sum_{p=1}^{P} s_p(t - q\tau T)e^{j2\pi f_p(t-\tau T)} + \eta_q^d(t) \\ &\approx \sum_{p=1}^{P} s_p(t)e^{j2\pi f_p t}e^{-j2\pi f_p \tau T} + \eta_q^d(t). \end{aligned} \quad (6)$$

The combined DTFT expression after sampling at f_s for all $N-1$ delay channels can be written as

$$\mathbf{X}_t(f) = \underbrace{[\mathbf{a}(f_1), \mathbf{a}(f_2), ..., \mathbf{a}(f_P)]}_{\mathbf{A}_t} \mathbf{S}(f) + \boldsymbol{\eta}^d(f) \quad (7)$$

where for any $1 \leq p \leq P$, $\mathbf{a}(f_p) = [1, e^{-j2\pi f_p \tau T}, e^{-j2\pi f_p 2\tau T}, \dots \ , e^{-j2\pi f_p (N-1)\tau T}]^{\mathcal{T}}$. In the following section we combine (5) and (7) and describe a method for generating a larger array referred as DST array.

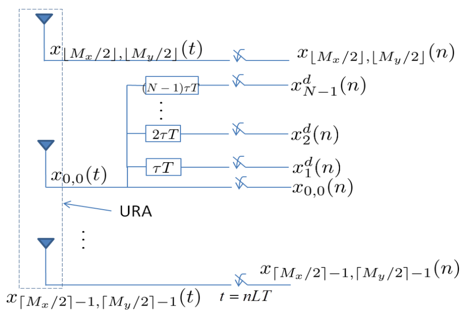

Fig. 1. Example of a multiple delay architecture considered in this paper. Notice that the delay channel network is added to the sensor placed at the origin.

B. Difference Space Time Array

Let the combined spatial and temporal delay network DTFT be represented by $\mathbf{X}_{st}(f) = [\mathbf{X}_s(f), \mathbf{X}_t(f)]^{\mathcal{T}}$. $\mathbf{X}_{st}(f)$ can be expressed as

$$\mathbf{X}_{st}(f) = \underbrace{\begin{pmatrix} \mathbf{A}_s \\ \mathbf{A}_t \end{pmatrix}}_{\mathbf{A}_{st}} \mathbf{S}(f) + \mathbf{N}(f). \tag{8}$$

Using the above equation, we form the following covariance matrix

$$\begin{aligned} \mathbf{R}_{xx}^{st} &= \int_{f\in\mathcal{F}} \mathbf{X}_{st}(f)\mathbf{X}_{st}^{H}(f)df \\ &= \mathbf{A}_{st} \underbrace{\left(\int_{f\in\mathcal{F}} \mathbf{S}(f)\mathbf{S}^{H}(f)df\right)}_{\mathbf{R}_{ss}} \mathbf{A}_{st}^{H} + \sigma_n^2\mathbf{I} \end{aligned} \tag{9}$$

where $\mathbf{R}_{ss}$ denotes the source covariance matrix. Due to the assumption of uncorrelated sources, $\mathbf{R}_{ss}$ will be a diagonal matrix with the elements captured by the vector $\boldsymbol{\lambda} = [\sigma_{s_1}^2, \sigma_{s_2}^2, ..., \sigma_{s_P}^2]^{\mathcal{T}}$, where $\sigma_{s_p}^2$ denotes the power of the p^{th} source. By vectorizing $\mathbf{R}_{xx}^{st}$, it can be expressed as

$$\begin{aligned} \mathbf{z} = \mathrm{vec}(\mathbf{R}_{xx}^{st}) &= (\mathbf{A}_{st}^{*} \otimes \mathbf{A}_{st})\mathrm{vec}(\mathbf{R}_{ss}) + \sigma_n^2\mathbf{1} \\ &= (\mathbf{A}_{st}^{*} \odot \mathbf{A}_{st})\boldsymbol{\lambda} + \sigma_n^2\mathbf{1} \\ &= \begin{pmatrix} \mathbf{A}_s^{*} \odot \mathbf{A}_t \\ \mathbf{A}_t^{*} \odot \mathbf{A}_s \\ \mathbf{A}_s^{*} \odot \mathbf{A}_s \\ \mathbf{A}_t^{*} \odot \mathbf{A}_t \end{pmatrix} \boldsymbol{\lambda} + \sigma_n^2\mathbf{1} \end{aligned} \tag{10}$$

where $'*'$ denotes the conjugate operation, $'\otimes'$ and $'\odot'$ denotes the Kronecker product and Khatri-Rao product respectively. The simplification from the Kronecker product to Khatri-Rao product is due to the diagonal structure of $\mathbf{R}_{ss}$. From the structure of $\mathbf{A}_{st}$, it can be observed that $(\mathbf{A}_{st}^{*} \odot \mathbf{A}_{st})$ contains rows corresponding to the *difference sensor locations* or in other words, $(\mathbf{A}_{st}^{*} \odot \mathbf{A}_{st})$ enumerates an array which we refer as difference array. Furthermore, it can be observed that difference array in general will be larger and would contain several virtual sensors. Let $\mathbf{z}_{m_x,m_y,m_\tau}^{dst}$ (m_x, m_y, m_τ denotes the sensor locations along the x, y and z-axis respectively) denote a subset of $\mathbf{z}$ corresponding to the rows of $(\mathbf{A}_s^{*} \odot \mathbf{A}_t)$ and $(\mathbf{A}_t^{*} \odot \mathbf{A}_s)$ which may be written as

$$\mathbf{z}_{m_x,m_y,m_\tau}^{dst} = \underbrace{\begin{pmatrix} \mathbf{A}_s^{*} \odot \mathbf{A}_t \\ \mathbf{A}_t^{*} \odot \mathbf{A}_s \end{pmatrix}}_{\mathbf{A}_{dst}} \boldsymbol{\lambda} + \sigma_n^2\mathbf{1}. \tag{11}$$

Recalling the symmetrical structure of URA (see (2)) and $\mathbf{A}_s = \mathbf{A}_x \odot \mathbf{A}_y$, it may easily be observed that $\mathbf{A}_{dst}$ enumerates a bigger *3-D uniform array* i.e., spatial delay due to URA along two dimensions and temporal delay along the third dimension. We refer to this 3-D uniform array as *difference space time array* (DST) whose sensor locations are given by $\mathcal{S}_{dst} =$

$$\begin{aligned} \{\mathbf{I}[dm_x \quad dm_y \quad \tau m_\tau], -\lfloor M_x/2 \rfloor \leq m_x \leq \lceil M_x/2 \rceil - 1, \\ -N \leq m_\tau \leq N, -\lfloor M_y/2 \rfloor \leq m_y \leq \lceil M_y/2 \rceil - 1\} \end{aligned} \tag{12}$$

An example of a DST array for $M_x = M_y = N = 3$ is shown in Fig. 2 . While the sensors indicated by blue depicts the actual sensors, sensors indicated by red indicates the virtual sensors. The bigger DST array compared to size of the actual physical sensing elements can clearly be noticed from the figure. It is to be noted that although $\mathbf{A}_{dst}$ is a bigger array, $\boldsymbol{\lambda}$ however is a column vector and hence the existing algorithms cannot be directly applied. Thus, in the following section, we present a new approach for estimating parameters with this bigger DST array.

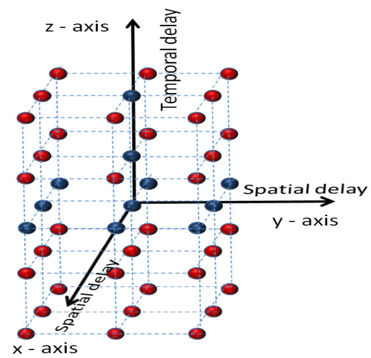

Fig. 2. Example of a DST for $M_x = M_y = N = 3$. Blue sensors shows the actual sensors, while the sensors shown in red depicts the virtual sensors.

C. Estimation algorithm

In this section, we first outline a 3-D rank enhancing algorithm based on the idea of spatial smoothing [15] and then describe an ESPRIT based algorithm capable of jointly estimating the frequencies and their corresponding 2-D DOAs.

1) Rank enhancing covariance matrix formulation: Let $\mathbf{A}_{dst} = \mathbf{A}_x^{dst} \odot \mathbf{A}_y^{dst} \odot \mathbf{A}_t$, where for $k = x$ and $k = y$, $\mathbf{A}_k^{dst}$ is of size $M_k^d \times P$, $M_k^d = \lceil M_k/2 \rceil$ and $[\mathbf{A}_k^{dst}]_{m_k,p} = e^{-j2\pi(d/c)(m_k-1)\omega_p^k}$. It is now easy to express $\mathbf{z}_{m_x,m_y,m_\tau}^{dst} = \mathbf{A}_{dst}\Delta_x^{m_x}\Delta_y^{m_y}\Delta_t^{m_t}\boldsymbol{\lambda}$, where $\Delta_x^{m_x}$, $\Delta_y^{m_y}$, $\Delta_t^{m_t}$ are diagonal matrices whose $(p,p)^{th}$ element is given by $e^{-j2\pi(d/c)m_x\omega_p^x}$, $e^{-j2\pi(d/c)m_y\omega_p^y}$ and $e^{-j2\pi m_t f_p \tau T}$ respectively. The rank enhanced covariance matrix of the DST can now be formed as $\mathbf{R}_{dst} =$

$$\sum_{m_x=-\lfloor M_x/4 \rfloor}^{\lceil M_x/4 \rceil - 1} \sum_{m_y=-\lfloor M_y/4 \rfloor}^{\lceil M_y/4 \rceil - 1} \sum_{m_\tau=-\lfloor N/2 \rfloor}^{\lceil N/2 \rceil - 1} \mathbf{z}_{m_x,m_y,m_\tau}^{dst} (\mathbf{z}_{m_x,m_y,m_\tau}^{dst})^{H} \tag{13}$$

2) Joint frequency and 2-D DOA estimation: We first determine the singular vectors $\mathbf{U}_s$ corresponding to the P largest singular values of $\mathbf{R}_{dst}$. In the noise-free setting it can easily be shown that $\mathbf{U}_s$ and $\mathbf{A}_{dst}$ spans the same subspace and hence $\mathbf{A}_{dst} = \mathbf{U}_s\boldsymbol{T}_R$, where $\boldsymbol{T}_R$ denotes a full rank transformation matrix of size $P \times P$.

Now, let us define the transformation matrices $\boldsymbol{\alpha}_l^f = [\mathbf{0} \quad \mathbf{I}_{N-1}]$, $\boldsymbol{\alpha}_r^f = [\mathbf{I}_{N-1} \quad \mathbf{0}] \in \mathbb{R}^{N-1\times N}$. Also defined are the transformation matrices $\boldsymbol{\alpha}_l^x$, $\boldsymbol{\alpha}_r^x \in \mathbb{R}^{M_x^d-1\times M_x^d}$, and $\boldsymbol{\alpha}_l^y$, $\boldsymbol{\alpha}_r^y \in \mathbb{R}^{M_y^d-1\times M_y^d}$ which are similar to $\boldsymbol{\alpha}_l^f$ and $\boldsymbol{\alpha}_r^f$. Further, let us define the following

$$\boldsymbol{\beta}_l^f = (\mathbf{I}_{M_x^d M_y^d} \otimes \boldsymbol{\alpha}_l^f) \in \mathbb{R}^{M_x^d M_y^d (N-1) \times M_x^d M_y^d N} \quad (14)$$
$$\boldsymbol{\beta}_r^f = (\mathbf{I}_{M_x^d M_y^d} \otimes \boldsymbol{\alpha}_r^f) \in \mathbb{R}^{M_x^d M_y^d (N-1) \times M_x^d M_y^d N} \quad (15)$$
$$\boldsymbol{\beta}_l^x = (\mathbf{I}_{M_y^d N} \otimes \boldsymbol{\alpha}_l^x) \in \mathbb{R}^{(M_x^d-1) M_y^d N \times M_x^d M_y^d N} \quad (16)$$
$$\boldsymbol{\beta}_r^x = (\mathbf{I}_{M_y^d N} \otimes \boldsymbol{\alpha}_r^x) \in \mathbb{R}^{(M_x^d-1) M_y^d N \times M_x^d M_y^d N} \quad (17)$$
$$\boldsymbol{\beta}_l^y = (\mathbf{I}_{M_x^d N} \otimes \boldsymbol{\alpha}_l^y) \in \mathbb{R}^{M_x^d (M_y^d-1) N \times M_x^d M_y^d N} \quad (18)$$
$$\boldsymbol{\beta}_r^y = (\mathbf{I}_{M_x^d N} \otimes \boldsymbol{\alpha}_r^y) \in \mathbb{R}^{M_x^d (M_y^d-1) N \times M_x^d M_y^d N} \quad (19)$$

where $\mathbf{I}_k$ denotes an identity matrix of order k. Now, using the above transformation matrices we can express the following relationships, $\boldsymbol{\beta}_l^f \mathbf{A}_{dst} = \boldsymbol{\beta}_r^f \mathbf{A}_{dst} \boldsymbol{\Omega}^f$, $\boldsymbol{\beta}_l^x \mathbf{A}_{dst} = \boldsymbol{\beta}_r^x \boldsymbol{\Pi}_1 \mathbf{A}_{st} \boldsymbol{\Omega}^x$ and $\boldsymbol{\beta}_l^y \mathbf{A}_{dst} = \boldsymbol{\beta}_r^y \boldsymbol{\Pi}_2 \mathbf{A}_{dst} \boldsymbol{\Omega}^y$. Here, $\boldsymbol{\Omega}^f = \text{diag}\{e^{-j2\pi f_1 \tau}, e^{-j2\pi f_2 \tau}, ..., e^{-j2\pi f_P \tau}\}$, $\boldsymbol{\Omega}^x = \text{diag}\{e^{j2\pi(d/c)\omega_1^x}, ..., e^{j2\pi(d/c)\omega_P^x}\}$, $\boldsymbol{\Omega}^y = \text{diag}\{e^{j2\pi(d/c)\omega_1^y}, ..., e^{j2\pi(d/c)\omega_P^y}\}$ and $\boldsymbol{\Pi}_1$, $\boldsymbol{\Pi}_2$ are permutation matrices such that for any matrices **A**,**B**,**C**, $\boldsymbol{\Pi}_1(\mathbf{A} \odot \mathbf{B} \odot \mathbf{C}) = \mathbf{B} \odot \mathbf{C} \odot \mathbf{A}$ and $\boldsymbol{\Pi}_2(\mathbf{A} \odot \mathbf{B} \odot \mathbf{C}) = \mathbf{C} \odot \mathbf{A} \odot \mathbf{B}$. Substituting $\mathbf{A}_{dst} = \mathbf{U}_s \boldsymbol{T}_R$ and simplifying, the above equations can be expressed as $\boldsymbol{\Psi}^f = (\boldsymbol{\beta}_r^f \mathbf{U}_s)^\dagger \boldsymbol{\beta}_l^f \mathbf{U}_s = \boldsymbol{T}_R \boldsymbol{\Omega}^f \boldsymbol{T}_R^{-1}$, $\boldsymbol{\Psi}^x = (\boldsymbol{\beta}_r^x \boldsymbol{\Pi}_1 \mathbf{U}_s)^\dagger \boldsymbol{\beta}_l^x \mathbf{U}_s = \boldsymbol{T}_R \boldsymbol{\Omega}^x \boldsymbol{T}_R^{-1}$ and $\boldsymbol{\Psi}^y = (\boldsymbol{\beta}_r^y \boldsymbol{\Pi}_2 \mathbf{U}_s)^\dagger \boldsymbol{\beta}_l^y \mathbf{U}_s = \boldsymbol{T}_R \boldsymbol{\Omega}^y \boldsymbol{T}_R^{-1}$. Since the transformation matrix of these equations are identical, by combining we can form the following equation

$$\boldsymbol{\Psi}^{(f,x,y)} = \boldsymbol{\Psi}^f + \boldsymbol{\Psi}^x + \boldsymbol{\Psi}^y = \boldsymbol{T}_R(\boldsymbol{\Omega}^f + \boldsymbol{\Omega}^x + \boldsymbol{\Omega}^y)\boldsymbol{T}_R^{-1}. \quad (20)$$

Now, it can easily be noticed that the eigenvectors of $\boldsymbol{\Psi}^{(f,x,y)}$ are nothing but the transformation matrix $\boldsymbol{T}_R$. Upon estimating this transformation matrix, $\boldsymbol{\Omega}^f, \boldsymbol{\Omega}^x$ and $\boldsymbol{\Omega}^y$ can be estimated with the same permutation order using $\boldsymbol{\Omega}^f = \boldsymbol{T}_R^{-1} \boldsymbol{\Psi}^f \boldsymbol{T}_R$, $\boldsymbol{\Omega}^x = \boldsymbol{T}_R^{-1} \boldsymbol{\Psi}^x \boldsymbol{T}_R$ and $\boldsymbol{\Omega}^y = \boldsymbol{T}_R^{-1} \boldsymbol{\Psi}^y \boldsymbol{T}_R$. The arguments of $\boldsymbol{\Omega}^f, \boldsymbol{\Omega}^x, \boldsymbol{\Omega}^y$ shall provide the triple $\{\hat{f}_p, \hat{\omega}_p^x, \hat{\omega}_p^y\}_{p=1}^P$ from which the frequencies and their 2D-DOAs can easily be estimated.

If in addition to the carrier frequencies and DOAs, signal $x(t)$ is required then by assuming $P \leq M + N - 1$, the array manifold matrix $\mathbf{A}_{st}$ can be formed with the estimated parameters and using (8), $\mathbf{S}(f)$ can be estimated, from which the the signal $x(t)$ can easily be determined.

D. Identifiability and minimum sampling rate

Proposition 3.1: With URA comprising of $M_x \times M_y$ sensors and a $N-1$ channel delay network outlined in Section III-A, and further assuming sources to be uncorrelated, the P carrier frequencies and their 2-D DOAs are recoverable *almost surely* (assuming no-noise) if

i) $L \leq 1/BT$

ii) $\omega_{p_1}^x \neq \omega_{p_2}^x + m, \omega_{p_1}^y \neq \omega_{p_2}^y + m, f_{p_1} \neq f_{p_2}$, for all $1 \leq p_1, p_2 \leq P, p_1 \neq p_2, m \in \mathbb{Z}$

iii) $P \leq \min\{M_x^d M_y^d (N-1), M_x^d (M_y^d - 1)N, (M_x^d - 1)M_y^d N\}$.

Due to lack of space, only a brief outline of proof is provided here. As mentioned earlier (refer (5)) that $S_p(f)$ is a periodic spectrum corresponding to the p^{th} source with period $f_s = 1/LT$. Since the bandwidth of $s_p(t)$ cannot exceed B, in order to avoid aliasing (i.e., $S_p(f + mf_s) \cap S_p(f + (m+1)f_s) = \emptyset, m \in \mathbb{Z}$), $f_s \geq B$ or $L \leq 1/BT$. For the ESPRIT algorithm, DST manifold matrix $\mathbf{A}_{dst}$ must be full rank. Since $\mathbf{A}_x^{dst}$, $\mathbf{A}_x^{dst}$ and $\mathbf{A}_t$ are Vandermonde matrices, if the second condition of the proposition is satisfied then by [16, Theorem 3], $\mathbf{A}_{dst}$ will be full rank *almost surely*. By observing the row-sizes of the transformation matrices (14) - (19), the maximum number of identifiable parameters can easily be proved. ■

Now, the first condition implies that a sampling frequency of $f_s \geq B$ would be sufficient and since the configuration consists of $M = M_x M_y$ sensors and $N-1$ channel delay network, the minimum overall sampling rate $f_{min}^{prop} = (M + N - 1)B$ and since $B \ll 1/T$, $f_{min}^{prop} \ll f_{nyq}$. With this minimum sampling rate assuming M_x and M_y to be even and $N < M_x^d M_y^d$, from third condition upto $P_{max} = M(N-1)/4$, i.e., $\mathcal{O}(MN/4)$ carrier frequencies and their 2-D DOAs can be estimated.

Most importantly, the limit provided here is for the extreme case when all the sources exactly alias to the same frequency. However, when the bands are separated (most often the case in practice), many more carrier frequencies and their DOAs can be estimated by applying the above approach to each individual filtered band. The following section corroborates these results through simulations.

IV. SIMULATION RESULTS

Simulations are performed to test the capability and performance of the proposed approach described in the previous sections. In all our simulations, we assume $\mathcal{F} = [0, 5]$ GHz, narrowband signal bandwidth $B = 10$ MHz, the number of sensor elements $M_x = M_y = 3$ and the delay factor $\tau = 0.5$. Further, for all the results presented here, we chose the extreme case where all the carrier frequencies exactly alias onto the same frequency due to sub-Nyquist sampling.

First, we conducted simulations to test the capability at minimum sampling rate as discussed in the previous section. To demonstrate this capability, we assumed $N = 10$ and $f_s = 10$ MHz. We fixed $P = 18$ since upto 18 carrier frequencies and their DOAs can be estimated with the chosen choice of the configuration (see Proposition 3.1). It is important to notice that since $f_s = B = 10$ MHz, all the bands will exactly alias between $[0, 10]$ MHz. A very high SNR of around 40dB was assumed for this simulation and Fig. 3 shows the actual and the estimated frequency and the 2-D DOAs (azimuth and elevation). The figure clearly shows that despite all the bands exactly aliased and $P > M$, the frequency and their 2-D DOAs are estimated with very good accuracy and are close to actual values (note that under noise-less condition the estimation will be exact).

Next, we conducted simulations to test the performance of the proposed approach. For this simulation we chose $P = 12$ and $f_s = 250$ MHz (i.e., downsampling factor $L = 20$). The carrier frequencies chosen were separated by a factor of 250 MHz, so that after sampling they all alias to the same frequency band. Due to space constraint, instead of providing separate performance plots corresponding to each of frequency and DOAs, since $P < M+N-1$, the combined

ISBN 978-0-9928626-7-1 © EURASIP 2017

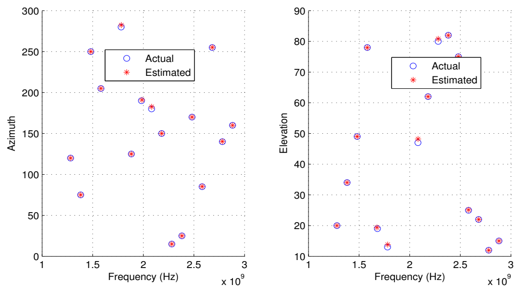

Fig. 3. Actual and estimated carrier frequencies and their 2-D DOAs for $P = 18$.

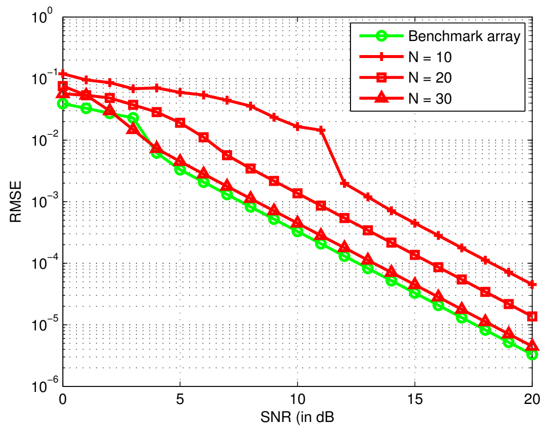

Fig. 4. Comparison of RMSE vs SNR for the reconstructed spectrum for different delay channels and the benchmark array.

reconstructed spectrum performance plot (as described in Section III) is provided. For the sake of comparison, the performance obtained with a benchmark array i.e., the space time array constructed by adding the $N-1$ channel delay network to *all the sensors* (hardware complexity same as that of [12]) is provided, which also serves as a good lower bound. Note that the same estimation algorithm as outlined in Section III-C2 (without the rank enhancement step) can be used for estimation on this benchmark array. Fig. 4 shows the root mean squared error (RMSE) performance of the proposed approach for different values of N and the benchmark array. For the benchmark array we have fixed $M_x = M_y = 3$ and $N = 10$. It is important to note that for this configuration, the benchmark array requires $M(N-1)$ channels (i.e., 81 channels) and operates on a covariance matrix of dimension 90×90, whereas the proposed approach requires only $M + N - 1$ $(9+N-1)$ channels and operates on a much smaller dimension of $M_x^d M_y^d N \times M_x^d M_y^d N$ (for this case it is $4N \times 4N$). The performance improvement with increase in N can clearly be noticed from the figure. In particular, observe that for $N = 30$ the performance is very close to the benchmark array. It is important to note the reduction of the overall sampling rate in addition to the reduction of the hardware and computation as mentioned above; while the overall sampling rate with the proposed approach is about 9.5 GHz (for $N = 30$), but with the benchmark array it requires about 20.25 GHz.

V. Conclusion

In this paper, a new scheme for joint frequency and 2-D DOA estimation at sub-Nyquist sampling rates using a standard URA comprising of $M = M_x \times M_y$ is presented. The receiver architecture is modified by adding an $N-1$ delay channel network to one element. By combining the URA and the delay channel network outputs a larger DST array is formed and a sub-space algorithm based on ESPRIT is presented. With this proposed approach, it is shown that one can jointly estimate $\mathcal{O}(MN/4)$ frequencies and their 2-D DOAs. These results are further verified through simulations. The advantage of the proposed scheme (as also demonstrated through simulations) can be leveraged to not only reduce the number of sensors but also to obtain huge savings in computation and in sampling rates.

References

[1] J. Mitola and G. Q. Maguire Jr, "Cognitive radio: making software radios more personal," *Personal Communications, IEEE*, vol. 6, no. 4, pp. 13–18, 1999.

[2] J. R. Guerci, *Space-time adaptive processing for radar*. Artech House, 2014.

[3] M. C. Vanderveen, A.-J. Van der Veen, and A. Paulraj, "Estimation of multipath parameters in wireless communications," *Signal Processing, IEEE Transactions on*, vol. 46, no. 3, pp. 682–690, 1998.

[4] D. Cohen, S. Tsiper, and Y. C. Eldar, "Analog to digital cognitive radio," in *Handbook of Cognitive Radio, 1st ed.,*. Springer, 2017.

[5] M. D. Zoltowski and C. P. Mathews, "Real-time frequency and 2-d angle estimation with sub-nyquist spatio-temporal sampling," *Signal Processing, IEEE Transactions on*, vol. 42, no. 10, pp. 2781–2794, 1994.

[6] S. Stein, O. Yair, D. Cohen, and Y. C. Eldar, "Joint spectrum sensing and direction of arrival recovery from sub-nyquist samples," in *Signal Processing Advances in Wireless Communications (SPAWC), 2015 IEEE 16th International Workshop on*. IEEE, 2015, pp. 331–335.

[7] A. A. Kumar, S. G. Razul, and C.-M. S. See, "Spectrum blind reconstruction and direction of arrival estimation of multi-band signals at sub-nyquist sampling rates," *Multidimensional Systems and Signal Processing*, pp. 1–27, 2016.

[8] ——, "Spectrum blind reconstruction and direction of arrival estimation at sub-nyquist sampling rates with uniform linear array," in *Digital Signal Processing (DSP), 2015 IEEE International Conference on*. IEEE, 2015, pp. 670–674.

[9] L. Liu and P. Wei, "Joint doa and frequency estimation with sub-nyquist sampling," *arXiv preprint arXiv:1604.05037*, 2016.

[10] A. A. Kumar, S. G. Razul, and C.-M. S. See, "Carrier frequency and direction of arrival estimation with nested sub-nyquist sensor array receiver," in *Signal Processing Conference (EUSIPCO), 2015 23rd European*. IEEE, 2015, pp. 1167–1171.

[11] D. D. Ariananda and G. Leus, "Compressive joint angular-frequency power spectrum estimation," in *Signal Processing Conference (EUSIPCO), 2013 Proceedings of the 21st European*. IEEE, 2013, pp. 1–5.

[12] L. Liu and P. Wei, "Joint doa and frequency estimation with sub-nyquist sampling for more sources than sensors," *arXiv preprint arXiv:1702.01386*, 2017.

[13] P. Pal and P. Vaidyanathan, "Nested arrays in two dimensions, part ii: Application in two dimensional array processing," *Signal Processing, IEEE Transactions on*, vol. 60, no. 9, pp. 4706–4718, 2012.

[14] M. Mishali and Y. C. Eldar, "Blind multiband signal reconstruction: Compressed sensing for analog signals," *Signal Processing, IEEE Transactions on*, vol. 57, no. 3, pp. 993–1009, 2009.

[15] L. C. Godara, "Application of antenna arrays to mobile communications. ii. beam-forming and direction-of-arrival considerations," *Proceedings of the IEEE*, vol. 85, no. 8, pp. 1195–1245, 1997.

[16] T. Jiang, N. D. Sidiropoulos, and J. M. ten Berge, "Almost-sure identifiability of multidimensional harmonic retrieval," *Signal Processing, IEEE Transactions on*, vol. 49, no. 9, pp. 1849–1859, 2001.

ISBN 978-0-9928626-7-1